Catalysis Letters
https://doi.org/10.1007/s10562-021-03735-0

Catalytic Ozonation of Quinoline Utilizing Manganese-Based Catalyst with Abundant Oxygen Vacancies

Liquan Xia[1,2,3] · Wenhui Liang[4] · Guifeng Chen[2,3] · Wenbo Li[2,3] · Minglong Gao[2,3]

Received: 18 March 2021 / Accepted: 8 July 2021

Abstract

S-MnO_2, Cl-MnO_2, and Ac-MnO_2 samples were prepared by redox method with the oxidant ($KMnO_4$) and the reducing agent precursors [$MnSO_4$, $MnCl_2$ and $Mn(Ac)_2$]. This work studied the influence of the precursors on the catalytic performance. Ac-MnO_2 was aminated and doped with graphene to obtain the modified manganese-based catalyst MnO_2-NH_2-GO. XRD, Raman, FTIR, XPS, NH_3-TPD, CV (cyclic voltammetry) were used to characterize the catalyst. The average oxidation state (AOS) of Mn element was also calculated. The results of the catalytic ozonation quinoline degradation experiment shown that the four catalysts was ranked as follows: S-MnO_2 < Cl-MnO_2 < Ac-MnO_2 < MnO_2-NH_2-GO, which was related to the catalyst crystal structure, oxygen vacancy (O_{vac})content, AOS, and catalyst surface acidity and other factors. The effects of CO_3^{2-}, HCO_3^-, SO_4^{2-}, and Cl^- on the catalytic reaction were investigated, the effects of different anions vary greatly. By adding tertiary butyl alcohol (tBA) and benzoquinone (pBQ) radical scavengers, it was confirmed that OH and O_2^- coexisted, but O_2^- contributed much more to oxidation than OH.

Graphic Abstract

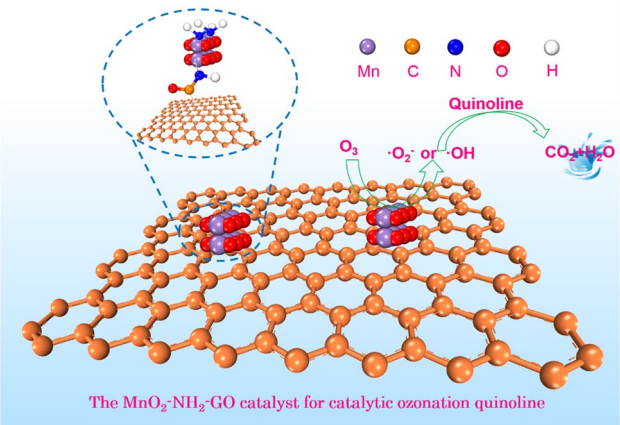

Keywords Precursor · MnO_2 · Oxygen vacancy · Catalytic oxidation · Quinoline

✉ Liquan Xia
331958435@qq.com

1 China Coal Research Institute, Beijing 100013, China

2 China Coal Research Institute Company Ltd., Beijing 100013, China

3 State Key Laboratory of Coal Mining and Clean Utilization, Beijing 100013, China

4 College of Life Science and Chemistry, Jiangsu Second Normal University, Nanjing 210013, China

1 Introduction

With the tightening of environmental protection policies, the improvement of laws and regulations, water treatment technology has been developed by leaps and bounds. However, there are still big challenges in the treatment of difficult-to-biodegradable industrial wastewater [1]. Heterogeneous catalytic ozonation (HCO) technology has been increasingly

Published online: 03 August 2021

used in wastewater treatment by its economic viability, no secondary pollution, and high salinity [2]. HCO technology mainly use active free radicals generated by ozone decomposition to degrade refractory organic, such as OH and O^{2-}, which have higher redox potential than ozone. Quinoline has important application in industrial and agricultural production. However, it is a typical refractory heterocyclic compound. In wastewater treatment technology, iron [3], manganese [4], copper [5], nickel [6] and other non-precious metal oxides were used as active components of the catalysts. And molecular sieves, natural minerals, carbon materials and other surface-rich carriers were used as a carrier of catalyst [7, 8]. Manganese-based catalysts have the advantages of cheap and easy to obtain and easy to adjust lattice defects. However, the research on the catalytic mechanism of manganese-based catalysts was not very thorough. According to the theory of HCO, the oxygen vacancy on the catalyst surface plays an important role in the reaction. Therefore, it is necessary to synthesize an efficient catalyst with abundant oxygen vacancy in order to effectively remove refractory organic from wastewater [9–11].

Literatures suggested that precursor anion will not participate in the chemical reaction, nor will it change the element composition of the manganese-based catalyst. However, different precursor anions have different effects on the structural characteristics of manganese-based catalysts [12]. Wang et al. [13] prepared manganese-based catalysts by redox method to change the types of anions under the premise of ensuring the same cation. The test results showed that when acetate was used as the precursor anion, the crystallinity of the prepared manganese oxide was the largest, and when the precursor anion was Cl^{-}, the crystallinity of the prepared manganese oxide was the smallest. Liu et al. [14] prepared supported catalysts by impregnation precipitation method, using three different anions of divalent manganese salts as precursors. The test results showed that when manganese acetate was selected as the precursor, the prepared catalyst had the largest specific surface area. The relationship between precursor anion and catalyst structure and catalytic ozonation performance is not clear.

Therefore, with the oxidant ($KMnO_4$) and the reducing agent precursors [$MnSO_4$, $MnCl_2$ and $Mn(Ac)_2$] under hydrothermal condition to prepare manganese-based catalysts. The performance of various catalysts was tested by catalytic ozonation of quinoline degradation, the relationship between catalyst structure and catalytic performance was analyzed from crystal defect, surface chemical state, bonding strength and so on. Average oxidation state (AOS) and oxygen vacancy content and catalytic performance, the mechanism between the three be studied. As a bridge between MnO_2 and GO, $–NH_2$ can improve the stability of the catalyst, and N atom can also increase the electron domain density on the surface of the catalyst. Graphene has a large specific surface area and good electrical conductivity, which can improve the electron transport efficiency of the catalyst after doping.

2 Experimental

2.1 Preparation of Catalyst

To study the effect of Mn(II) precursor on the catalytic organic degradation, the MnO_2 catalysts were prepared by a hydrothermal synthesis between potassium permanganate ($KMnO_4$) and manganese acetate [$Mn(CH_3COO)_2{\cdot}4H_2O$], manganese chloride ($MnCl_2{\cdot}4H_2O$), or manganese sulfate ($MnSO_4{\cdot}H_2O$). Note that all the chemicals used in this study were of analytical grade, and were used without further purification. The process was as follows:the Mn(II) precursor solution was dropped into the $KMnO_4$ solution under vigorous stirring 30 min, then in hydrothermal synthesis reactor 140 °C for 12 h, filtered and washed three times with deionized water. The obtained solid sample was dried at 105 °C for 12 h. and followed by the sample was grinded to powder (40–60 mesh). These synthesized samples were donated as Ac-MnO_2 (manganese acetate as precursor),Cl-MnO_2 (manganese chloride as precursor) and S-MnO_2 (manganese sulfate as pre-cursor).Ac-MnO_2 mixes with toluene, add 3-aminopropyltriethoxysilane and GO, ultrasonic processing 30 min, then in hydrothermal synthesis reactor 140 °C for 12 h, washing and drying the product. The synthesized samples were donated as MnO_2-NH_2-GO.

2.2 Catalyst Characterization

The X-ray diffraction (XRD) patterns of the catalyst were obtained on an X-ray diffract meter (D/max-2500/PC X-ray diffractometer of Rigaku Corporation), with Cu Kα as the radiation source, and the tube voltage was 40 kV, 40 mA. The scanning range of the tube current is 10–80° in step of 0.01°/s. X-ray photoelectron spectroscopy (XPS, American Physical Electronics, PHI5300) is used to analyze the elements and their valence information on the catalyst surface. The data obtained is processed by XPS-PEAK software for peak splitting, and the molar ratio of the elements is determined by the area ratio after splitting. The NH_3-TPD is used for testing the surface acidity, the atmosphere is 10% NH_3/Ar mixed gas, the temperature is programmed at 5℃/min, and the absorption peak is detected in the range of 50–800℃; Raman (Horiba HR-800) is used for testing the Me–O(Me: metal) structure, the range of wavenumber 100–2000 cm^{-1}, and the excitation light source was Ar^{+} (532 nm). Fourier transform infrared spectroscopy (FTIR, Thermo, IS50) was used to further characterize the functional groups on the catalyst surface, scan and record the absorption peak in the

wavenumber range of 100–2000 cm^{-1}.The electrochemical performance was studied by cycli voltammetry(CV, Autolab 302 N electrochemical workstation) with charge–discharge cycling.

2.3 Catalytic Ozonation

The performance of the catalyst was evaluated in a fixed bed reactor, the process diagram is shown in Fig. S1. The complex redox reaction occurs between ozone, quinoline solution ($C_0 = 50$ mg/L) and the catalyst (0.5 g/L) under agitation. Take samples every ten minutes and use high performance liquid chromatography (HLCP, Waters, USA) to detect the quinoline concentration and calculate the removal rate. The UV detector with detection wavelength of 313 nm, methanol–water solution (3:2,v/v) as the mobile phase, and a flow rate of 1.0 ml min^{-1}.

3 Results and Discussion

3.1 Catalyst Characterization

XRD analysis is usually used to determine crystal composition and crystallize parameters of catalysts. The structure of MnO_2 that synthesized from different precursors were analyzed by XRD as shown in Fig. 1a. It can be observed that the peak positions of MnO_2 are similar but the peak intensities differ greatly. The crystal structure of Cl-MnO_2 and Ac-MnO_2 are very similar. Both belong to α-MnO_2. Specific surface area, pore structure distribution, surface chemical state, catalytic oxidation performance and other indicators of α-MnO_2 are all better than other crystal types of MnO_2 [15]. But in this study, it is found that Cl-MnO_2 has a lower yield. This may be caused by part of the Cl^- and Mn^{2+} competing with the oxidant, and worse, it may produce toxic and harmful Cl_2 [16]. Martins et al. [17] observed that Mn(III) acetate was significantly more stable than Mn(III) chloride which would indicate a thermodynamic favourability in the kinetics of oxidizing the acetate versus the sulfate. A stable intermediate Mn(III) species will increase the forward reaction rate producing Mn(IV) as the final product. In addition, it can be observed that Ac-MnO_2 owned weaker diffractions than other samples, suggesting lower crystallinity which benefits the ozonation. The higher crystallinity, the fewer the lattice defects of the catalyst. In the experiment of catalytic ozonation quinoline degradation, defects on the catalyst surface are often reflected as active sites, so too high crystallinity is not conducive to catalytic reaction [18, 19]. In addition, higher crystallinity will increase the internal resistance of the catalyst and reduce electron transport efficiency [20].

Cyclic voltammetry (CV) curves of MnO_2 composite electrodes are depicted in Fig. 1b. The spectrum shown that each catalyst has two peaks, which can be attributed to oxidation of anode Mn^{3+} and reduction of cathode Mn^{4+}, respectively, the shapes of the CV curves exhibit more or less pronounced redox waves. This behavior suggests that faradic phenomena occur during the charge-storage mechanism. The redox peaks may reflect the redox transitions of Mn between different valence states, including Mn^{3+}/Mn^{4+} and Mn^{4+}/Mn^{3+}. It can be observed from the figure that the intensity of various peaks gradually decreases in the following order: Ac-MnO_2 > Cl-MnO_2 > S-MnO_2.This is consistent with the AOS calculation results below, according to AOS calculation formula the lower AOS indicates a higher Mn^{3+}/Mn^{4+} value. Therefore, Ac-MnO2 will have stronger oxidation/reduction peaks [21].

The Fourier infrared spectrum in Fig. 2a clearly shown the absorption peaks of various catalysts. A large number

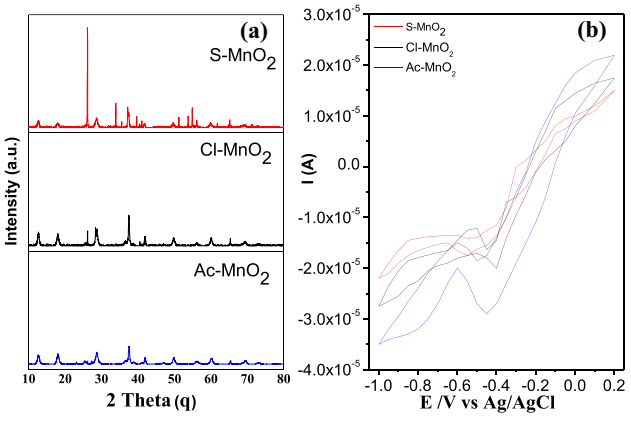

Fig. 1 XRD patterns (**a**) and cyclic voltammetry scans (**b**) of different MnO_2

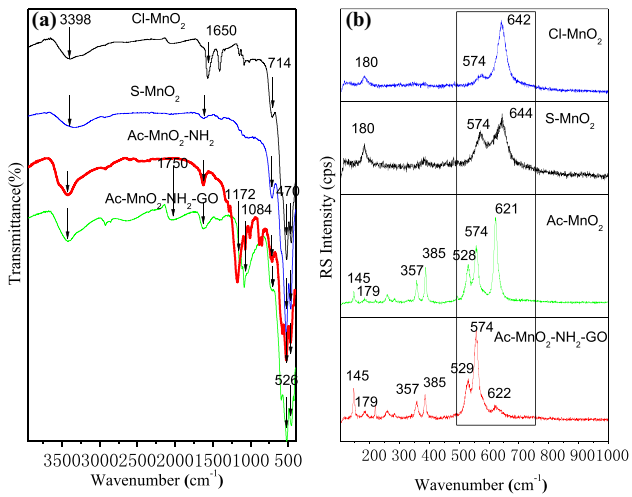

Fig. 2 FTIR spectra (**a**) and Raman spectra (**b**) of different catalyst

of strong absorption peaks appear near the wave number of 500 cm^{-1}, which can be attributed to Mn–O. Because the Mn–O bond has both raman activity and infrared activity, strong absorption peaks appear in both characterizations, which mutually confirm the fact that Mn–O exists [22]. The absorption peak at the wave number of 1750 cm^{-1} can be attributed to the stretching vibration of the hydroxyl group (–OH). The peak intensity of Ac-MnO_2-NH_2-GO is significantly greater than Ac-MnO_2-NH_2, indicating that there is a large amount of –OH on the surface of Ac-MnO_2-NH_2-GO. According to the mechanism of ozone degradation, the –OH on the surface of catalyst is one of active sites for generating active free radicals, so –OH is positively correlated with the catalytic activity [23]. The infrared characteristic peaks of N–H are 1172 cm^{-1} and 3398 cm^{-1}. Compared with other MnO_2, the vibration peak intensity of MnO_2-NH_2 at 3358 cm^{-1} has been significantly improved, and a new vibration peak appears at position 1172 for MnO_2-NH_2, indicating that the amino group was successfully grafted onto the surface of manganese dioxide. Compared with MnO_2-NH_2, the vibration peak intensity of MnO_2-NH_2-GO at 1172 and 3398 cm^{-1} was significantly reduced, indicating that GO was successfully compounded with MnO_2 through chemical bonding with amino groups. After dopeing GO, a strong absorption peak appears at 1084 cm^{-1}, which can be attributed to the stretching vibration of C–N, indicating that the C atom in GO forms a bond with the N in the –NH_2, which is beneficial to the improvement of electron transport efficiency [24].

The Raman spectra of these catalysts are shown in Fig. 2b, the Raman signal at 500–700 cm^{-1}, which is considered to be the fingerprint region of manganese dioxides, corresponding diffraction peak are attributed to the vibration of MnO_6 octahedron. Cl-MnO_2 has characteristic vibration peaks at 642 and 574 cm^{-1}, which are attributed to the A_g vibration mode. The previous peak is attributed to the Mn–O in MnO_6 tensile vibration, the latter belongs to MnO_6 octahedral symmetrical tensile vibration [25, 26]. S-MnO_2 has characteristic vibration peaks at 644 and 574 cm^{-1}, which also belong to the A_g vibration mode. However, the amplitude of Mn–O vibration is much smaller than that of Cl-MnO_2, and the symmetrical tensile vibration of MnO_6 octahedron is obviously stronger, indicating that the Mn–O in S-MnO_2 is stronger, which is consistent with the XRD results. During catalytic ozonation, ozone reacted with particular Mn–O bonds to generate more powerful oxygen species, leading to better oxidation efficiency compared to single ozonation. Therefore, strong Mn–O bond leads to poor mobility of oxygen on the catalyst surface, which is not conducive to the activation of ozone. Compared with the former catalysts, Ac-MnO_2 vibration peak position is significantly weaker, and characteristic vibration peaks appear at 621 and 568 cm^{-1}, but the former peak is significantly, and the intensity of the latter peak is significantly reduced. According to the quantum theory of raman spectroscopy, the interaction between molecules and laser radiation can be analyzed from the perspective of energy transfer [27]·The obvious changes in the peak show that the formation of oxygen vacancies will change the spatial structure of MnO_6 octahedrons [28, 29].

Considering the vital impact of Mn–O bond on the catalytic activity, the AOS of surface Mn element was analyzed via XPS. As shown in Fig. 3a, XPS spectrum of $Mn2p_{2/3}$ has two peaks at the positions where the binding energy is 641.5 eV and 642.7 eV. They are classified as characteristic peaks of Mn^{3+} and Mn^{4+} [30]. According to the principle of conservation of charge when Mn^{3+} exists in MnO_2, in

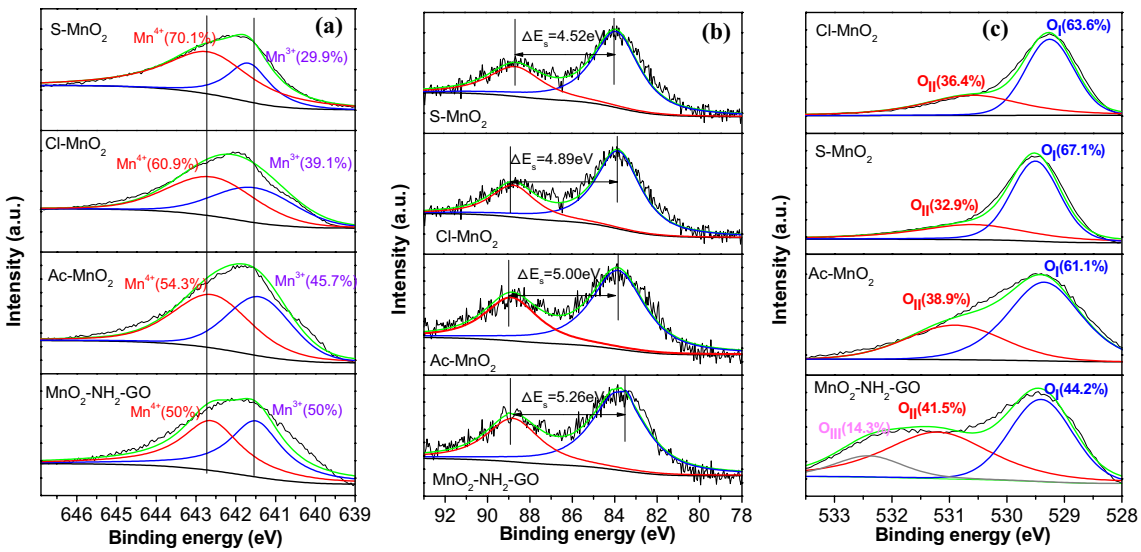

Fig. 3 XPS spectra of Mn $2p_{2/3}$ (**a**), Mn 3 s (**b**) and O1s (**c**) of different catalyst

order to maintain charge balance, oxygen vacancies will be generated through formula (1). Compared with the lattice oxygen, oxygen vacancies have higher mobility, oxygen vacancies are conducive to electron transfer to improve the catalytic performance. It can be seen from Table 1 that different Mn(II) precursors have a greater impact on Mn^{3+}/Mn^{4+} in MnO_2, and the ranking is: S-MnO_2(0.429) < Cl-MnO_2(0.639) < Ac-MnO_2(0.842) < MnO_2-NH_2-GO(1.00). The higher ratio of Mn^{3+}/Mn^{4+}, the higher content of Mn^{3+} in MnO_2. High concentration Mn^{3+} in the tunnel can expand crystal cell and break the charge balance, leading to a lower AOS of Mn, which means abundant oxygen vacancy. Therefore, we can infer that Ac-MnO_2 with high concentration oxygen vacancies. According to the reaction mechanism that oxygen vacancies participate in the decomposition of ozone to generate free radicals, the abundant oxygen vacancies on the catalyst surface will cause ozone molecules to rapidly convert into O_2 and other free active oxygen [31].

$$4Mn^{4+} + O^{2-} \rightarrow 4Mn^{4+} + 2e^-/v_o + 1/2O_2 \rightarrow 2Mn^{4+} + 2Mn^{3+} + v_o + 1/2O_2 \quad (1)$$

AOS can truly reflect the valence state information of MnO_2, and it can usually be measured by thiosulfate titration or voltammetric electrochemical titration [32]. In this work, following formula AOS = 8.956–1.126ΔEs (ΔEs:the binding energy between the two main peaks of Mn) to calculate AOS [33]. Mn3s spectra of different precursor synthesis catalysts are shown in Fig. 3b. The results show that the AOS of Mn on the catalyst surface decreases in the following order: S-MnO_2 (3.87) > Cl-MnO_2 (3.45) > Ac-MnO_2 (3.33) > MnO_2-NH_2-GO (3.03), meaning a lower average coordination number and higher oxygen vacancy content of MnO_2-NH_2-GO. In addition, the decrease of AOS means that Jahn–Teller (JT) distortion can occur to lower the system ground state which has the same conclusion with XRD results.

O1s spectrum on the surface of the catalyst is divided into peaks. The binding energy around 531.0 eV can be attributed to adsorbed oxygen (O_{II}:O_2^{2-}, O^{2-}, O^-, –OH), and the lattice oxygen (O_I:O_2^-) with binding energy around 529.7 eV. Both surface oxygens of the catalyst can affect the catalytic ozonation of organic degradation. Recent literature shows that: compared with lattice oxygen, surface adsorbed oxygen has better fluidity and supplements lattice oxygen through a series of migration and transformation [34]. As shown in Fig. 3c and Table 1, the ratio of O_{II}/O_I with a significant difference in various catalysts, the order is as following: S-MnO_2(0.490) < Cl-MnO_2(0.572) < Ac-MnO_2(0.631) < MnO_2-NH_2-GO(0.939), this result was consistent with the splitting result of Mn2p. This is because the surface adsorbed oxygen are often adsorbed in the oxygen vacancies on the catalyst surface, O_{II}/O_I has a greater relationship with the oxygen vacancy content. In addition, the specific surface area, pore structure and adsorption performance of the catalyst were greatly improved after modification. The specific results are shown in Table S1, and the adsorption performance is shown in Figure S2.

As a typical porous material, graphene can not only provide a rich specific surface area, but also increase the electron transport efficiency of the redox process. After the modification of MnO_2, various properties showed a significant improvement, results are shown in Table 1. Some researches reveal that enhanced chemical bonds between graphene and active constituents not only improve the electrochemical performance of composites, but also strengthen the bonding between constituents [35, 36].

The literature has proposed the ozone decomposition steps [37]. However, the active site for ozone decomposition on the MnO_2 surface is still unknown. Catalytic ozonation of organic degradation is related to a number of closely related processes and is not determined by a certain condition. The process of catalyzing ozonation the degradation of organic can be roughly described as follows: firstly, ozone is adsorbed and activated on the surface of the catalyst (the functional groups such as the hydroxyl groups on the surface of the catalyst will chemically interact with ozone to enhance the adsorption of ozone); then, the oxygen vacancies on the surface of MnO_2 participate in the ozone decomposition produces free radicals; finally, the active free radicals achieve no-selection and high-efficiency degradation of organic pollutants. The acidic sites on the catalyst

Table 1 Statistical results of catalyst characterization

Catalyst	NH_3 consumption (mmol/g)	Mn^{3+}/Mn^{4+}	O_{II}/O_I	AOS	O_{vac} content	K/Mn
S-MnO_2	0.898	0.429	0.490	3.870	0.015	0.100
Cl-MnO_2	2.077	0.639	0.572	3.450	0.187	0.176
Ac-MnO_2	2.077	0.842	0.631	3.330	0.238	0.074
MnO_2-NH_2-GO	1.982	1.00	0.939	3.030	0.455	0.060

surface can effectively adsorb ozone, so the acidic sites have an important influence on the catalytic oxidation process.

The NH_3-TPD technology was used to characterize the acidic sites on the catalyst surface, results are shown in Fig. 4. Binding strength of acid sites and NH_3 molecules is positively correlated with desorption temperature. It can be observed that the desorption spectra of three MnO_2 are relatively similar, but there are big differences in the curve area. The specific data in Table 1, the curve integral area as following: S-MnO_2 < Ac-MnO_2 < Cl-MnO_2. The total acidity of S-MnO_2 is the smallest, indicating abundant sites on its surface, its peak position is 341℃, and the strength of the acidic sites is also poor.Ac-MnO_2 consumes NH_3 relatively close to Cl-MnO_2. However, the peak position of Ac-MnO_2 is at 365 °C, which is much higher than the 343 °C of Cl-MnO_2, so the acidic site of Ac-MnO_2 has a stronger bond with NH_3. In addition, Ac-MnO_2 also appeared desorption peaks at lower temperatures, indicating that Ac-MnO_2 has more weak acid sites. The desorption peaks of MnO_2-NH_2-GO and Ac-MnO_2 are very similar, but the former consumes less NH_3. This due to the functional groups on the GO surface occupying some acidic sites. The catalytic process is a complex heterogeneous reaction, catalytic effect is affected by many factors [38].

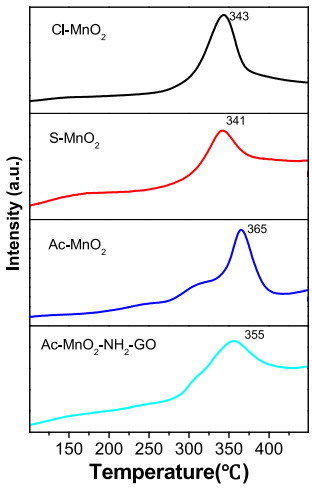

Fig. 4 NH_3-TPD spectra of different materials

3.2 Catalytic Ozonation of Quinoline

3.2.1 Influence of Mn(II) Precursor

The results of the quinoline degradation experiment are shown in Fig. 5. The catalytic performance of manganese-based catalysts synthesized by different precursors are quite different, and the catalytic effect of S-MnO_2 is the worst: quinoline removal rate of 75.12% can only be achieved after 60 min of reaction. However, in the Ac-MnO_2 catalyzed reaction system, a removal rate of over 88% can be achieved in 60 min. Cl-MnO_2 catalytic system after 60 min of reaction, it can achieve a quinoline degradation rate of 82.9%. This is mainly due to the fact that the catalyst synthesized by $Mn(Ac)_2$ as a precursor has more surface oxygen vacancies, lower AOS, more surface acid sites, and weaker Mn–O bonding. According to the degradation mechanism of organic, these performance parameters of catalyst are very important for catalytic degradation of

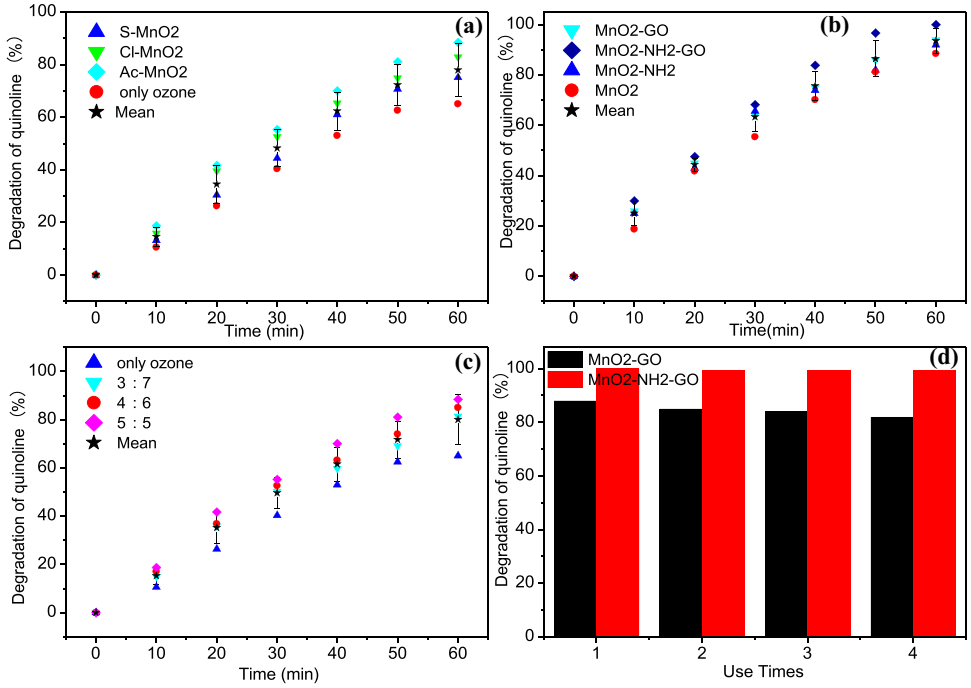

Fig. 5 The influence of different precursors (**a**) different ratios of $KMnO_4$: $MnAc_2{\cdot}4H_2O$ (**b**) and the performance of the modified catalyst (**c**) results of multiple times reuse (**d**) (Reaction conditions: 0.5 g catalyst/L, Ozone 10 mg /min, C_0 = 50 mg/L)

organic. The experimental results are consistent with the reaction principle and characterization results, the catalytic activity order of the there samples decreased as follows: Ac-MnO_2 > Cl-MnO_2 > S-MnO_2.

For catalytic oxidation of organic pollutants, byproducts are critical results The byproducts formation after catalytic ozonation be characterized and analyzed in detail. Part of the characterization results are shown in Figure S6. The degradation products are mainly quinoline derivatives and organic acids. Combined with the conclusions of previous studies, organic acids are relatively difficult to mineralize organics and are an important reason for the high COD content of wastewater. In addition, combining quinoline degradation intermediate products and literature data, the possible degradation path of quinoline is deduced, as shown in Figure S8.

3.2.2 Influence of Feed Ratios

It can be seen from Fig. 5b that when the catalyst is also prepared with $Mn(Ac)_2$ and $KMnO_4$ as precursors, different reaction ratios have a greater impact on the catalytic performance of the catalyst. Literature show that the influence of different reactant ratios on the catalyst mainly affects the crystal structure, and the bond length, bond angle and pore structure of Mn–O in different phases of MnO_2 are quite different. In the redox reaction to produce MnO_2, MnOOH or Mn_2O_3 are more likely to be produced when oxidants are insufficient. XRD analysis of MnO_2, which prepared with different oxidant and reducing agent ratios, the results are shown in Figure S4.When Mn^{7+}: Mn^{2+} = 5:5, the crystal of MnO_2 is closest to the α-MnO_2, it can be seen from Figure S4 that α-MnO_2 has the lowest crystallinity and there are more active sites exposed: (110), (200), (310), (211), (301), (411) and (512) crystal plane, facilitate the flow of surface oxygen. Which are conducive to the progress of the catalytic reaction [39], the degradation effect of quinoline was consistent with that in Fig. 5b. When Mn^{7+}: Mn^{2+} = 3:7, the crystalline form of MnO_2 belongs to β-type, after 60 min of reaction, the removal rate of quinoline decreased from 88 to 80.5%. The previous research results of our research group shown that β-MnO_2 has the highest AOS, that is, less oxygen vacancies at this time are not conducive to the ozonation. The catalytic activity order of the three samples decreased as follows: MnO_2 (5:5) > Cl-MnO_2 (4:6) > S-MnO_2 (3:7).

3.2.3 Catalyst Modification

Considering the catalytic effect and preparation cost of the catalyst, Ac-MnO_2 was selected as the modified object for amination and graphene doping. It can be seen from Fig. 5c that the amination of Ac-MnO_2 to prepare MnO_2-NH_2 and the MnO_2-GO prepared after doping with GO can slightly improve the performance of the catalyst. Then, comparing MnO_2-NH_2-GO with MnO_2 alone, it can be found that after 60 min of reaction, the removal rate of quinoline increased from 88 to 99.9%, the performance of the modified catalyst is greatly improved.

The experimental result of repeated use is shown in Fig. 5d. It can be observed that: compared with MnO_2-GO, the modified catalyst MnO_2-NH_2-GO has better catalytic activity after repeated use for four times. This may be because –NH_2 acts as a bridging bond to enhance the bonding between GO and MnO_2, build a bridge between graphene and metal oxide to strengthen the bond between graphene and metal oxide. The amino group (–NH_2) can form a covalent chemical bond with the oxygen-containing functional group on the surface of the graphene. At the same time, it can also form a covalent chemical bond with the metal oxide(MeO) formation –N-Me-chemical bond increasing the oxygen vacancy content of the catalyst and also enhancing the electron transport efficiency of the redox reaction process [40]. The electro-chemical impedance spectroscopies (EIS) of MnO_2-NH_2-GO and MnO_2-GO are shown in Fig. S3. The arc radius of MnO_2 shows MnO_2-GO Nyquist plot becomes larger after second use and third use, indicating a depravation of electronic conductivity and a deactivation between MnO_2 and GO. On the contrary, MnO_2-NH_2-GO for catalytic ozonation, the four arc radii almost converge to one point. That is, the electronic conductivity of MnO_2-NH_2-GO keeps pretty stable, suggesting a strong bonding between MnO_2 and GO has been established in MnO_2 has been established in MnO_2-NH_2-GO.

3.2.4 The Influence of Inorganic Anions

Industrial wastewater contains various inorganic anions, which may have a serious impact on the degradation of organic [41]. To provide a theoretical basis for future engineering applications, 500 mg/L of inorganic anions were added to the reaction system to investigate the influence of the anions on the reaction effect. It can be observed from Fig. 6a that inorganic anions have varying degrees of influence on the effect of catalytic ozonation. Cl^- and HCO_3^-, as typical capture agents of OH radicals, will react with free radicals to reduce the catalytic effect [42, 43]. The degradation efficiency of quinoline from 99.9 to 91.24% and 93.92%, respectively, after adding a certain amount of hydrogen carbonate and chlorine ions. In general, inorganic anions have little effect on the catalytic ozonation and degradation of organics. In industrial production, the targeted reduction of Cl^- and HCO_3^- content in the previous section can effectively avoid the problem of reduced catalytic effect. This series of experimental results provide guidance for industrial applications.

In order to explore the types of free radicals in the catalytic reaction process, tBA was used as a trap for ·OH and

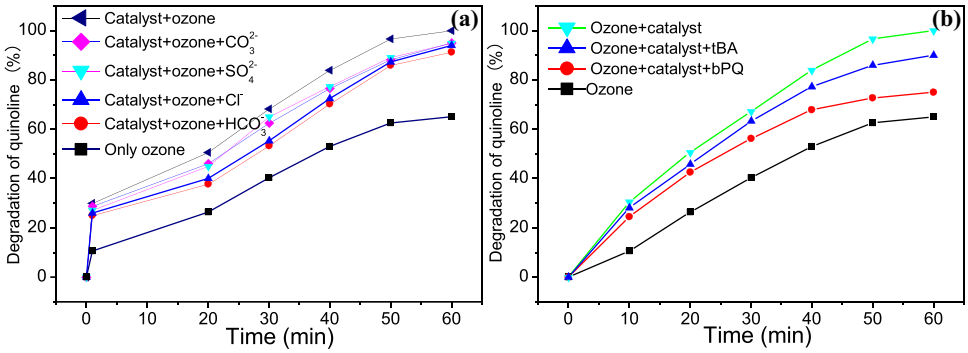

Fig. 6 The influence of inorganic anions (**a**) and free radical inhibitors (**b**) on catalytic performance (Reaction conditions: 0.5 g catalyst/L, Ozone 10 mg / min, C_0 = 50 mg/L)

bPQ as a trap for superoxy radicals (O_2^-) [5]. The experimental results are shown in Fig. 6b. It can be clearly seen from the figure that the addition of bPQ will significantly reduce the catalytic effect of catalysis. After 60 min, the degradation rate of quinoline will be reduced from 99.9 to 75.0%, addition of tBA at the same concentration, the degradation effect of quinoline was 90.1% after 60 min. It can be inferred from this that in the process of catalytic ozonation, there are two kinds of radicals, OH and O_2^-, but the contribution of O_2^- is much greater than that of OH.

4 Conclusion

Three kinds of MnO_2 are prepared with different precursors. The experimental results shown that the performance of catalysts prepared by different Mn^{2+} precursors is quite different. Ac-MnO_2 has the best catalytic performance, with highest content of oxygen vacancies, lowest AOS, and most acidic sites. Quinoline can achieve a degradation rate of over 88% after 60 min. After the catalyst is modified, the stability and electron transport efficiency of the catalyst are effectively improved, especially the oxygen vacancy content on the surface of the catalyst was greatly increased. The free radical verification test showed that: O_2^- contribution to the degradation of quinoline is much greater than OH, so the active free oxygen mainly participates in the reaction of organic mineralization in the form of O_2^-. By combining the characterization data with the experimental results of oxidation, we can draw a conclusion that the oxygen vacancy content of catalyst is positively correlated with its catalytic performance.

Supplementary Information The online version contains supplementary material available at https://doi.org/10.1007/s10562-021-03735-0.

Acknowledgements This project was supported by National Key R&D Program of China (2019YFE0103300).

Declarations

Conflict of interest All authors declare that no conflict of interest exists.

References

1. Chen CM, Yoza BA, Wang YD et al (2015) Catalytic ozonation of petroleum refinery wastewater utilizing Mn-Fe-Cu/Al_2O_3 catalyst. Environ Sci Pollut Res 22:5552–5562
2. Zhuang HF, Han HJ, Jia SY et al (2014) Advanced treatment of biologically pretreated coal gasification wastewater by a novel integration of heterogeneous catalytic ozonation and biological process. Bioresour Tech 166:592–599
3. Fatma G, Özkan G, Belgin G (2019) Degradation of chloramphenicol and metronidazole by electro-fenton process using graphene oxide-Fe_3O_4 as heterogeneous catalyst. J Environ Chem Eng 7:102990–102997
4. Wang YX, Xie YB, Sun HQ (2016) 2D/2D nano-hybrids of γ-MnO_2 on reduced graphene oxide for catalytic ozonation and coupling peroxymono sulfate activation. J Hazard Mater 301:56–64
5. Liu D, Wang CR, Song YF (2019) Effective mineralization of quinoline and bio-treated coking wastewater by catalytic ozonation using $CuFe_2O_4$/sepiolite catalyst: efficiency and mechanism. Chemosphere 227:647–656
6. Wang YZ, Zhu YT, Liu Z et al (2019) Catalytic performances of Ni-based catalysts on supercritical water gasification of phenol solutionand coal-gasification wastewater. Int J Hydrog Energy 44:3470–3480
7. Descorme C (2017) Catalytic wastewater treatment: oxidation and reduction processes recent studies on chlorophenols. Catal Today 297:324–334
8. Li XH, Chen WY, Ma LM et al (2019) Characteristics and mechanisms of catalytic ozonation with Fe-shaving-based catalyst in industrial wastewater advanced treatment. J Clean Prod 222:174–181
9. Xu J, Li Yu, Qian MQ et al (2019) Amino-functionalized synthesis of MnO_2-NH_2-GO for catalytic ozonation of cephalexin. Appl Catal B 256:117797
10. Li CH, Jiang F, Sun DZ et al (2017) Catalytic ozonation for advanced treatment of incineration leachate using (MnO_2-Co_3O_4)/AC as a catalyst. Chem Eng J 325:624–631

11. Nawaz F, Cao HB, Xie YB et al (2017) Selection of active phase of MnO_2 for catalytic ozonation of 4-nitrophenol. Chemosphere 168:1457–1466
12. Ly Y, Li CT, Du XY (2020) Catalytic oxidation of toluene over MnO_2 catalysts with different Mn(II) precursors and the study of reaction pathway. Fuel 262:116610
13. Wang G, Zhang J, Zhou J, Qian G (2019) Production of an effective catalyst with increased oxygen vacancies from manganese slag for selective catalytic reduction of nitricoxide. J Environ Manage 23:990–995
14. Boyjoo Y, Rochard G, Giraudon JM et al (2018) Mesoporous MnO_2 hollow spheres for enhanced catalytic oxidationof formaldehyde. Sustain Mater Technol 17:e00091
15. Zhu GX, Zhu JG, Jiang WJ (2017) Surface oxygen vacancy induced α-MnO_2 nanofiber for highlyefficient ozone elimination. Appl Catal B 209:729–737
16. Yang YJ, Jia JB, Liu Y et al (2018) The effect of tungsten doping on the catalytic activity of α-MnO_2 nanomaterial for ozone decomposition under humid condition. Appl Catal A 562:132–141
17. Martins RC, Quinta-Ferreira RM (2009) Catalytic ozonation ofphenolic acids over a Mn−Ce−O catalyst. Appl Catal B 90(1):268–277
18. Wang Y, Chen L, Cao H et al (2019) Role of oxygen vacancies and Mn sites in hierarchical Mn_2O_3/$LaMnO_{3-\delta}$ perovskite composites for aqueous organic pollutants decontamination. Appl Catal B 245:546–554
19. Valdeś H, Tardoń RF, Zaror CA (2012) Role of surface hydroxyl groups of acid-treated natural zeolite on the heterogeneous catalytic ozonation of methylene blue contaminated waters. Chem Eng J 211–212:388–395
20. Niu Z, Yue T, Hu WH et al (2019) Covalent bonding of MnO_2 onto graphene aerogel forwards: efficiently catalytic degradation of organic wastewater. Appl Surf Sci 496:543–585
21. Faheem N, Xie YB, Xiao JD et al (2016) The influence of the substituent on the phenol oxidation rate and reactive species in cubic MnO_2 catalytic ozonation. Catal Sci Technol 6:7875–7881
22. Li C, Wang JG, Zhang C et al (2019) Boosting acetone oxidation efficiency over MnO_2 nanorods by tailoring crystal phases. New J Chem 43:19126–19131
23. Moulavi MH, Kale BB, Bankard D et al (2019) Green synthetic methodology: an evaluative study for impact of surfacebasicity of MnO_2 doped MgO nanocomposites in wittig reaction. J Solid State Chem 269:167–174
24. Amr HM, Marjorie LB, Dirk T et al (2019) Heterogeneous activation of peroxymono sulfate by a novel magnetic 3D γ-MnO_2@$ZnFe_2O_4$/rGO nanohybrid as a robust catalyst for phenol degradation. Appl Catal B 244:946–956
25. Jia JB, Yang WJ, Zhang PY et al (2017) Facile synthesis of Fe-modified manganese oxide with high content of oxygen vacancies for efficient airborne ozone destruction. Appl Catal A 546:79–86
26. Liu Y, Zhou H, Cao RR (2019) Facile and green synthetic strategy of birnessite-type MnO_2 with high efficiency for airborne benzene removal at low temperatures. Appl Catal B 245:569–582
27. Esmailpour AA (2019) Promoting surface oxygen vacancies on ceria via light pretreatment to enhance catalytic ozonation. Catal Sci Technol 9:5979
28. Ma Y, Gao W, Zhang Z et al (2018) Regulating the surface of nanoceria and its applications in heterogeneous catalysis. Surf Sci Rep 73(02):1–36
29. Aškrabić ZD, Dohčević VD, Araújo GI et al (2013) F-centre luminescence in nanocrystalline CeO_2. J Phys D 46:495306
30. Song C, Guo BB, Sun XF (2019) Enrichment and degradation of tetracycline using three-dimensional graphene/MnO_2 composites. Chem Eng J 358:1139–1146
31. Peng X, Guo Y, Yin Q et al (2017) Double-exchange effect in two-dimensional MnO_2 nanomaterials. J Am Chem Soc 139(14):5242–5248
32. Yang Y, Huang J, Wang S et al (2013) Catalytic removal of gaseous unintentional POPs on manganese oxide octahedral molecular sieves. Appl Catal B 142:568–578
33. Mo SP, Zhang Q, Li JQ et al (2020) Highly efficient mesoporous MnO_2 catalysts for the total toluene oxidation: oxygen-vacancy defect engineering and involved intermediates using in situ DRIFTS. App Catal 264:118–124
34. Jiang Y, Wei M, Feng J et al (2016) Enhancing the cycling stability of Na-ion batteries by bonding SnS_2 ultrafine nanocrystals on amino-functionalized graphene-hybrid nanosheets. Energy Environ Sci 9:1430–1438
35. Meng X, Yu C, Song X et al (2018) Scrutinizing defects and defect density of selenium-doped graphene for high-efficiency triiodide reduction in dye-sensitized solar cells. Angew Chem Int Ed 57(17):4682–4686
36. Zhu GX, Zhu JG, Li WL et al (2018) Tuning the K^+ concentration in the tunnels of α-MnO_2 to increasethe content of oxygen vacancy for ozone elimination. Environ Sci Technol 52:8684–8692
37. Esmailpour A, Moradi S, Yun J (2019) Promoting surface oxygen vacancies on ceria via light pretreatment to enhance catalytic ozonation. Catal Sci Technol 9:5979
38. Zhang T, Li WW, Jean PC (2011) Catalytic ozonation of oxalate with a cerium supported palladium oxide: an efficient degradation not relying on hydroxyl radical oxidation. Environ Sci Technol 45:9339–9346
39. Zhao H, Dong YM, Jiang PP et al (2014) An α-MnO_2 nanotube used as a novel catalyst in ozonation: performance and the mechanism. New J Chem 38:17–27
40. Yu GF, Wang YX, Cao HB et al (2020) Reactive oxygen species and catalytic active sites in heterogeneous catalytic ozonation for water Purification. Environ Sci Technol 54:5931–5946
41. Wang YZ, Wang SZ, Guo Y et al (2012) Oxidative degradation of lurgi coal-gasification wastewater with Mn_2O_3, Co_2O_3, and CuO catalysts in supercritical water. Ind Eng Chem Res 51:16573–16579
42. Wang JL, Chen H (2020) Catalytic ozonation for water and wastewater treatment: recent advances and perspective. Sci Total Environ 704:1–14
43. Zhu H, Ma WC, Han HJ et al (2017) Catalytic ozonation of quinoline using nano-MgO: Efficacy, pathways, mechanisms and its application to real biologically pretreated coal gasification wastewater. Chem Eng J 327:91–99